Optimization of classical nonpolarizable force fields for OH− and H3O+

Douwe Jan Bonthuis, Shavkat I. Mamatkulov, and Roland R. Netz

Citation: The Journal of Chemical Physics **144**, 104503 (2016); doi: 10.1063/1.4942771
View online: http://dx.doi.org/10.1063/1.4942771
View Table of Contents: http://scitation.aip.org/content/aip/journal/jcp/144/10?ver=pdfcov
Published by the AIP Publishing

Optimization of classical nonpolarizable force fields for OH^- and H_3O^+

Douwe Jan Bonthuis,[1,a] Shavkat I. Mamatkulov,[2] and Roland R. Netz[3]
[1]*Rudolf Peierls Centre for Theoretical Physics, University of Oxford, Oxford OX1 3NP, United Kingdom*
[2]*Ion-Plasma and Laser Technologies Institute of the Uzbekistan AS, Tashkent, Uzbekistan*
[3]*Fachbereich Physik, Freie Universität Berlin, 14195 Berlin, Germany*

(Received 10 September 2015; accepted 11 February 2016; published online 8 March 2016)

We optimize force fields for H_3O^+ and OH^- that reproduce the experimental solvation free energies and the activities of $H_3O^+Cl^-$ and Na^+OH^- solutions up to concentrations of 1.5 mol/l. The force fields are optimized with respect to the partial charge on the hydrogen atoms and the Lennard-Jones parameters of the oxygen atoms. Remarkably, the partial charge on the hydrogen atom of the optimized H_3O^+ force field is $0.8 \pm 0.1|e|$—significantly higher than the value typically used for nonpolarizable water models and H_3O^+ force fields. In contrast, the optimal partial charge on the hydrogen atom of OH^- turns out to be zero. Standard combination rules can be used for $H_3O^+Cl^-$ solutions, while for Na^+OH^- solutions, we need to significantly increase the effective anion-cation Lennard-Jones radius. While highlighting the importance of intramolecular electrostatics, our results show that it is possible to generate thermodynamically consistent force fields without using atomic polarizability. © *2016 AIP Publishing LLC.* [http://dx.doi.org/10.1063/1.4942771]

I. INTRODUCTION

It is difficult to overstate the importance of H_3O^+ and OH^- in chemistry and biology. For example, any chemical reaction in aqueous solution that involves gaining or losing a proton is pH dependent. The pH dependence of surface charge densities, which control the behavior of colloids in water—and therefore most biological interactions—is particularly strong.[1,2] In biology, protons have a special importance because proton gradients, which serve as an intermediate for energy storage in mitochondria, are being considered as the origin of complex life.[3] Nevertheless, there are still many remaining questions surrounding the properties of H_3O^+ and OH^- in water, such as the molecular origin of their high mobility and their surface activity.[4–6]

The success of the simple rigid water model SPC/E (Simple Point Charge/Extended),[7] that has neither molecular nor atomic polarizability, at reproducing water properties is remarkable. Most notably, the water's structure factor and dielectric response function are captured accurately based on the careful optimization of the Lennard-Jones (LJ) parameters and partial charges only.[8,9] Also for monovalent and divalent ions, optimization of the LJ parameters and combination rules suffices to reproduce solvation free energy, solvation enthalpy, and activity coefficients,[10–12] as well as density, isothermal compressibility, and solution activity as a function of salt concentration,[13,14] and cation-specific binding onto protein surface charges.[15] In contrast, similar force fields for the water ions have been lacking up to now. Yet without such force fields, thermodynamically consistent simulations of H_3O^+ and OH^- in water are out of reach.

In this paper, we report the optimization of nonpolarizable atomistic force fields for H_3O^+ and OH^- based on their solvation free energies and the thermodynamic activities of $H_3O^+Cl^-$ and Na^+OH^- solutions. We perform thermodynamic integrations for different values of the LJ parameters σ_i and ϵ_i of the oxygen and the partial charge δ_i on the hydrogen atoms to calculate the solvation free energy, where i denotes the ion type (H_3O^+ or OH^-). For each value of δ_i, this provides us with a curve in $\sigma_i - \epsilon_i$ space along which the experimental solvation free energy is reproduced. Along these isolines, we calculate the logarithmic derivative of the activity with respect to the concentration using Kirkwood-Buff theory. We find an optimal force field for H_3O^+ by varying δ_i, ϵ_i, and σ_i. For OH^-, we also need to modify the combination rule for the effective Na^+–OH^- LJ radius. Note that we do not intend to propose a microscopic model of, e.g., the charge distributions or the sizes of H_3O^+ and OH^- ions. Instead, our aim is to develop force fields that reproduce the ions' thermodynamic properties—in particular, their solvation free energies and thermodynamic activities. This ensures a correct binding strength of hydration water, as well as realistic effective interionic interactions. With two experimental reference quantities, the system is underdetermined. However, the sensitivity of these quantities to the force field parameters—especially to δ_i—is so strong that we are able to determine unique force fields for both H_3O^+ and OH^- with a margin for δ_i of only $0.1e$. We check the transferability of our optimized force fields by comparison with experimental data for the dielectric constant and the mass densities of aqueous Na^+OH^- and $H_3O^+Cl^-$ solutions, and find good agreement.

II. LITERATURE FORCE FIELDS

Many different force fields for H_3O^+ and OH^- have been proposed in the literature. Most force fields have either flexible bond lengths or flexible angles or both, atomic polarizability or virtual LJ sites, and the geometric structure of the different models varies widely. Listing all possible combinations would

[a]Electronic mail: douwe.bonthuis@physics.ox.ac.uk

TABLE I. The partial charge δ_i on the hydrogen atom of ion i, or on a virtual site close to the hydrogen atom, for several force fields used in the literature.

Ion	δ_i ($\|e\|$)	Remarks	Reference
H_3O^+	0.585	Flexible angles	16,17
	0.424	Double Coulomb/LJ site for oxygen	18
	1.26	With one additional virtual LJ site	19
	0.4722	With atomic polarizability	6,20
	0.4606	Flexible angles and bond lengths	21
	0.416	Rigid molecule	22
OH^-	0.23	Split Coulomb/LJ site for hydrogen, double Coulomb/LJ site for oxygen, and 5 additional virtual LJ sites	18
	0.32	Rigid molecule	17
	0.35	With atomic polarizability	6,20

be too exhaustive, but as for water models, the most important characteristic for the thermodynamic properties of the ions is the distribution of the partial charges. To give an impression of the typical charge distributions used, we list the values of the partial charge on the hydrogen atoms δ_i in terms of the elementary charge e of several literature force fields in Table I. Note that partial charges on the other atomic sites complement the partial charges on the hydrogen atom to attain the ion's net charge. With one notable exception, $\delta_{H_3O^+}$ is close to the value used for water ($\delta_{H_2O} = 0.4238$ for SPC/E), while δ_{OH^-} is slightly lower.

III. EXPERIMENTAL REFERENCE VALUES

A. Experimental values of the solvation free energy

Experimentally, the solvation free energy of ions can only be measured for neutral pairs. To determine the energy for a single ion, a reference ion has to be chosen, for which traditionally the proton H^+ is used. Estimates of the solvation free energy of the proton, however, vary between −1056 kJ/mol[23] and −1104.5 kJ/mol.[24] To circumvent this discrepancy, we use the difference in solvation free energy between the ion in question and chloride, for which some consensus exists regarding its force field parameters.[10] We calculate the energy of transfer of an ion from the 1 atm gas phase to the 1 mol/l liquid phase. The solvation free energy of H_3O^+ is calculated using the following thermodynamic cycle:

$$\begin{array}{ccccc} 2\,H_2O_{gas} & \overset{\Delta G_{gas}}{\longrightarrow} & OH^-_{gas} & + & H_3O^+_{gas} \\ \uparrow -2\Delta G_{H_2O} & & \downarrow \Delta G_{OH^-} & & \downarrow \Delta G_{H_3O^+} \\ 2\,H_2O_{aq} & \overset{-\Delta G_{aq}}{\longleftarrow} & OH^-_{aq} & + & H_3O^+_{aq}. \end{array} \quad (1)$$

The gas phase reaction energy $\Delta G_{gas} = \Delta^f G_{H_3O^+} + \Delta^f G_{OH^-} - 2\Delta^f G_{H_2O}$ can be estimated from the standard Gibbs free energies of formation in the ideal gas phase at a pressure of 0.1 MPa and a temperature of 298 K, $\Delta^f G_{H_2O} = -228.6$ kJ/mol, $\Delta^f G_{H_3O^+} = 606.6$ kJ/mol and $\Delta^f G_{OH^-} = -138.7$ kJ/mol,[25] giving $\Delta G_{gas} = 925.1$ kJ/mol. This value has been disputed, however, and we use a value of $\Delta G_{gas} = 945.6$ kJ/mol, which is considered to be more accurate.[26–28] To calculate the reaction energy in the liquid phase, ΔG_{aq}, we use

$$\exp\left(\frac{-\Delta G_{aq}}{k_B T}\right) = \frac{[OH^-]_{aq}[H_3O^+]_{aq}}{[H_2O]^2_{aq}}, \quad (2)$$

where [. . .] denotes activity. Activity coefficients for H_3O^+ and OH^- are assumed to be 1 because of the low concentrations involved, leading to $[OH^-]_{aq} = [H_3O^+]_{aq} = 10^{-7}$ mol/l. Since the H_2O concentration is not close to zero, the activity of pure water with respect to the 1 mol/l reference state cannot be assumed to be 1, but the water activity will be canceled out in the final expression, as we will show later. We find $\Delta G_{aq} = 2k_BT \ln [H_2O]_{aq} + 79.9$ kJ/mol. The Gibbs free energy of solvation of water ΔG_{H_2O} is obtained from the relation

$$\exp\left(\frac{-\Delta G_{H_2O}}{k_B T}\right) = \frac{[H_2O]_{aq}}{[H_2O]_{gas}}. \quad (3)$$

The activity of saturated water vapor at $T = 298$ K equals $[H_2O]_{gas} = 1.27 \cdot 10^{-3}$ mol/l,[29] again assuming an activity coefficient of 1. Eq. (3) gives $\Delta G_{H_2O} = -k_BT \ln [H_2O]_{aq} - 16.5$ kJ/mol, for going from the 1 mol/l gas state to the 1 mol/l liquid state. To go from the 1 atm standard state to the 1 mol/l liquid state, 7.9 kJ/mol has to be added.[30]

From the cycle in Eq. (1), we derive $\Delta G_{H_3O^+} + \Delta G_{OH^-} = \Delta G_{aq} + 2\Delta G_{H_2O} - \Delta G_{gas} = -882.9$ kJ/mol. Using the experimental values from Tissandier[24] for $\Delta\Delta G_{OH^-} = \Delta G_{H^+OH^-} - \Delta G_{H^+Cl^-}$, and using $\Delta G_{H^+OH^-} = \Delta G_{H^+} + \Delta G_{OH^-}$ and $\Delta G_{H^+Cl^-} = \Delta G_{H^+} + \Delta G_{Cl^-}$, we find

$$\begin{aligned} \Delta\Delta G_{OH^-} &= \Delta G_{OH^-} - \Delta G_{Cl^-} = -126.6 \text{ kJ/mol}, \\ \Sigma\Delta G_{H_3O^+} &= \Delta G_{H_3O^+} + \Delta G_{Cl^-} = -756.3 \text{ kJ/mol}. \end{aligned} \quad (4)$$

These values agree within several kJ/mol with the values given by Ref. 27: $\Delta\Delta G_{OH^-} = -126.7$ kJ/mol and $\Sigma\Delta G_{H_3O^+} = -758.6$ kJ/mol. Note that the values mentioned in Ref. 27 correspond to the transfer of an ion from 1 mol/l gas to 1 mol/l liquid, so 7.9 kJ/mol has been added to the solvation energy of each ion to compare to our values.

B. Experimental values of the activity derivative

To optimize the force fields with respect to the activity coefficient, we use the mean activity coefficients of HCl and NaOH solutions. From the numerical derivatives of the curves of the mean activity coefficient γ versus salt concentration n given by Refs. 31 and 32, we find at $n = 1.0$ mol/l,

$$\left.\frac{\partial \ln \gamma}{\partial \ln n}\right|_{NaOH} = 0.02 \quad \text{and} \quad \left.\frac{\partial \ln \gamma}{\partial \ln n}\right|_{HCl} = 0.18, \quad (5)$$

in agreement with the values given in Ref. 33.

IV. MOLECULAR DYNAMICS SIMULATIONS

A. Geometric structure of the hydronium and hydroxide ions

For the OH^- and H_3O^+ ions, we use the model sketched in Fig. 1. The partial charge on the hydrogen atom is denoted by δ_i. Hydronium has a trigonal pyramidal shape. The minimum

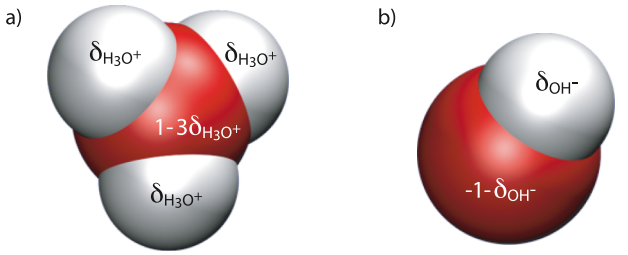

FIG. 1. Schematic images of (a) a hydronium and (b) a hydroxide ion. Partial charges q are indicated in terms of the partial charge $\delta_{H_3O^+}$ and δ_{OH^-} on the hydrogen atoms.

energy structure estimated from *ab initio* calculations for an isolated H_3O^+ ion has a H–O–H angle of 112.5°,[34] which has been used in earlier H_3O^+ force fields.[6] However, the actual angle of an isolated H_3O^+ ion is estimated to be 110°–112°,[34] and diode laser spectroscopy measurements yield an angle of 111.3° in the gas phase.[35] Following Ref. 20, we employ an angle of 111.4°, which is achieved by constraining the H–H bond to 0.1619 nm. The O–H bond length is set to 0.98 Å for H_3O^+[6,20,34,35] and 1.0 Å for OH^-.[6,20] All distances within the ions are constrained in our simulations.

B. Thermodynamic integration

We perform thermodynamic integrations to calculate the solvation free energies of H_3O^+ and OH^- by atomistic molecular dynamics simulation using the GROMACS package.[36] Each thermodynamic integration is carried out in two steps. First, the energy resulting from the LJ interaction is calculated by creating a neutral sphere with only LJ interactions. Second, the sphere is charged to calculate the energy resulting from the Coulomb interaction. Creation and charging of the particle take place by perturbing the interaction potential along a path parameterized by the coupling parameters λ_{LJ} and λ_{c}, respectively. The perturbed interaction potential V_{ij}^{λ} between two particles i and j, located a distance r_{ij} apart, is given by

$$V_{ij}^{\lambda} = \frac{\lambda_{\text{c}} q_i q_j}{4\pi\epsilon_0 r_{ij}} + 4\epsilon_{ij}\lambda_{\text{LJ}}\left[\left(\frac{\sigma_{ij}}{r_{ij}}\right)^{12} - \left(\frac{\sigma_{ij}}{r_{ij}}\right)^{6}\right], \tag{6}$$

with q_i and q_j being the unperturbed partial charges, and σ_{ij} and ϵ_{ij} being the unperturbed LJ diameter and interaction energy, respectively. The Hamiltonian H_λ used for the molecular dynamics equals the sum of the kinetic energy and the potential energy,

$$H_\lambda(\lambda_{\text{LJ}}, \lambda_{\text{c}}) = \sum_{i=1}^{N} \frac{m_i v_i^2}{2} + \sum_{i<j}^{N} V_{ij}^{\lambda}(r_{ij}), \tag{7}$$

with m_i being the particle's mass and v_i being its velocity. The solvation free energy is calculated from the integral

$$\Delta G = \int_0^1 \left\langle \frac{\partial H_\lambda(\lambda_{\text{LJ}}, 0)}{\partial \lambda_{\text{LJ}}} \right\rangle \mathrm{d}\lambda_{\text{LJ}} + \int_0^1 \left\langle \frac{\partial H_\lambda(1, \lambda_{\text{c}})}{\partial \lambda_{\text{c}}} \right\rangle \mathrm{d}\lambda_{\text{c}}, \tag{8}$$

where $\langle \ldots \rangle$ denotes the ensemble average, which is approximated by the time average. The integrations are performed for the interaction parameters of a single molecule. The two integrals in Eq. (8) are performed in two separate steps over a 12-point Gaussian sequence along the solvation path, $\lambda_i \in \{0.009\,22, 0.047\,94, 0.115\,05, 0.260\,634, 0.316\,08, 0.437\,38, 0.562\,62, 0.683\,92, 0.793\,66, 0.884\,95, 0.952\,06, 0.990\,78\}$.

C. Correction terms

The combination of Ewald summation and periodic boundary conditions necessitates removal of the energy due to long-ranged electrostatic interactions between the primary simulation box and its periodic images. This first correction term can be split into two parts.[37] The first part corresponds to the interaction energy of the ion with its own periodic images in a vacuum,

$$\Delta G_{fl} = -\frac{e^2}{8\pi\varepsilon_0}\frac{\xi}{R}, \tag{9}$$

with R being the size of the simulation box and ε_0 being the permittivity of the vacuum. The prefactor of the Wigner energy per particle on a cubic lattice equals $\xi = -2.837\,297$.[38] The second part corresponds to the effect of the periodic images of the ion on the solvent, which for spherical ions of radius r_a equals

$$\Delta G_{f2} = \frac{e^2(\varepsilon - 1)}{8\pi\varepsilon\varepsilon_0 R}\left[\xi + \frac{4\pi}{3}\left(\frac{r_a}{R}\right)^2 - \frac{16\pi^2}{45}\left(\frac{r_a}{R}\right)^5\right], \tag{10}$$

with $\varepsilon = 71$ being the dielectric constant of bulk SPC/E water.[39] The sum of Eqs. (9) and (10) gives the finite-size correction term $\Delta G_f = \Delta G_{fl} + \Delta G_{f2}$,

$$\Delta G_f = \frac{e^2(\varepsilon - 1)}{6\varepsilon\varepsilon_0 R}\left[\left(\frac{r_a}{R}\right)^2 - \frac{4\pi}{15}\left(\frac{r_a}{R}\right)^5\right] - \frac{e^2\xi}{8\pi\varepsilon\varepsilon_0 R}. \tag{11}$$

Strictly speaking, these equations are not precisely applicable because the hydronium and hydroxide ions have partial charges. In this case, the finite-size correction comprises an extra term corresponding to the interaction of each partial charge with the periodic images of the other partial charges. The terms due to the ion size r_a will be more complicated for non-spherical ions. For our system, however, Eq. (11) equals around 2 kJ/mol, and any modification of the correction will have an even smaller effect. Therefore, we use Eq. (11) in our optimization.

The experimental solvation free energies of Eq. (4) refer to a hypothetical transfer from a 1 atm ideal gas phase into a 1 mol/l ideal solution. Therefore, we add a second correction term corresponding to the compression free energy of an ideal gas from a pressure of $p_0 = 1$ atm to a pressure of $p_1 = k_{\text{B}} T\, n N_{\text{A}} \cdot 10^3$, which is the pressure in Pascal at a concentration of n, with N_{A} being Avogadro's number,

$$\Delta G_p = k_{\text{B}} T \ln(p_1/p_0). \tag{12}$$

Using $n = 1$ mol/l, we find $p_1 = 24.6$ atm and $\Delta G_p = 7.9$ kJ/mol.

The third correction term corresponds to the energy required to bring an ion from a vacuum to bulk water. Passing the interface potential ψ_s of the water, consisting of dipolar and quadrupolar terms,[40] requires an energy of

$$\Delta G_s = ze\psi_s. \tag{13}$$

The value of the interface potential is highly debated. A value of $\psi_s = -0.527$ V has been found in simulations with the

TIP4Q-FQ water force field,[41] which has been used in earlier force field optimizations.[10] For SPC/E, the interface potential has been found to be $\psi_s = -0.546$ V[42] or $\psi_s = -0.600$ V.[43] Apart from the system size and the real-space cutoff length for the electrostatics, the difference between these simulations is the cutoff length used for the LJ interaction, 10 Å[42] versus 8 Å.[43] In the original SPC/E optimization, a cutoff radius of 9 Å was used.[7] As we employ a cutoff radius of 10 Å, we use $\psi_s = -0.546$, leading to $\Delta G_s = -52.7$ kJ/mol. Note that ΔG_s does not affect the optimization because we use the solvation free energy sum of positive and negative ions or the difference between negative ions.

Finally, long-ranged dispersion interactions lead to an extra correction term, which may need to be included if different force fields have been derived using different cutoff schemes. For a homogeneous fluid with N heterogeneous LJ sites, the energy correction equals[44]

$$G_{\mathrm{LRC}} = \frac{16\,\pi\rho}{N-1}\sum_{i<j}\left(\frac{\epsilon_{ij}\sigma_{ij}^{12}}{9\,r_c^9} - \frac{\epsilon_{ij}\sigma_{ij}^{6}}{3\,r_c^3}\right), \tag{14}$$

with r_c being the LJ cutoff radius and ρ being the average density of the pure solvent. The direct contribution of the long-ranged interaction correction to the solvation free energy is calculated analytically from the difference between only water and water with one added ion using Eq. (14). For our system, the correction ΔG_{LRC} amounts to 0.5 kJ/mol at most, and is therefore neglected in the calculations.

D. Kirkwood-Buff integration

Optimization of the force fields with respect to the solvation free energies yields curves in $\sigma_i - \epsilon_i$ space. Along these free energy isolines, we optimize the force fields with respect to the activity coefficient of ion pairs. Using charge neutrality, the monovalent ion density $n = n_+ = n_-$ can be expressed in terms of Kirkwood-Buff integrals $G^\infty_{\alpha\beta}$ as $n = (G^\infty_{+-} - G^\infty_{++})^{-1}$.[45] Therefore, the logarithmic derivative of the activity with respect to n equals the following combination of Kirkwood-Buff integrals:[45]

$$a_{cc} = 1 + \frac{\partial \ln \gamma}{\partial \ln n} = \frac{G^\infty_{+-} - G^\infty_{++}}{2\,(G^\infty_{+-} - G^\infty_{+s})}. \tag{15}$$

The subscripts +, −, and s denote cation, anion, and solvent, respectively, and γ denotes the mean activity coefficient of anions and cations. In Eq. (15), $G^\infty_{\alpha\beta}$ is the integral of the excess pair correlation functions of the species α and β over infinite space, given by the $R \to \infty$ limit of the expression[46]

$$G^R_{\alpha\beta}(R) = \frac{1}{v\,(R)}\int_{v(R)}\int_{v(R)}\left[g_{\alpha\beta}(\boldsymbol{r}_1,\boldsymbol{r}_2) - 1\right]\mathrm{d}\boldsymbol{r}_1\mathrm{d}\boldsymbol{r}_2, \tag{16}$$

with $g_{\alpha\beta}(\boldsymbol{r}_1,\boldsymbol{r}_2)$ being the pair correlation function. Both integrals in Eq. (16) are performed over the spherical volume $v\,(R) = \frac{4}{3}\pi R^3$. In a homogeneous isotropic fluid, the pair correlation function can be written as $g_{\alpha\beta}(\boldsymbol{r}_1,\boldsymbol{r}_2) = g_{\alpha\beta}(|\boldsymbol{r}_1 - \boldsymbol{r}_2|)$. Therefore, the double integral in Eq. (16) can be reduced to a single integral over the radial coordinate r using a geometrical weight function $w\,(r,R)$, which differs from $4\pi r^2$ for finite R,[47]

$$G^R_{\alpha\beta}(R) = \int_0^{2R} w\,(r,R)\left[g_{\alpha\beta}(r) - 1\right]\mathrm{d}r, \tag{17}$$

with

$$\begin{aligned} w\,(r,R) &= \frac{1}{v\,(R)}\int_{v(R)}\int_{v(R)}\delta\left(r - |\boldsymbol{r}_1 - \boldsymbol{r}_2|\right)\,\mathrm{d}\boldsymbol{r}_1\mathrm{d}\boldsymbol{r}_2 \\ &= 4\pi r^2\left[1 - \frac{3\,r}{4R} + \frac{r^3}{16R^3}\right]. \end{aligned} \tag{18}$$

The upper integration limit in Eq. (17) comes from the fact that $|\boldsymbol{r}_1 - \boldsymbol{r}_2| \le 2R$. The difference between $G^\infty_{\alpha\beta}$ and $G^R_{\alpha\beta}(R)$ in Eq. (17) scales linearly with $1/R$,[47] which enables us to calculate $G^\infty_{\alpha\beta}$, including uncertainty, by extrapolating Eq. (17) to infinite box size.

E. Simulation details

1. Thermodynamic integration

For the thermodynamic integration in GROMACS, we use stochastic dynamics simulations.[36] We use a simulation box filled with 506 SPC/E molecules, apart from a handful of simulations where we use 2580 SPC/E molecules to check for finite-size effects. We use periodic boundary conditions in all directions and geometric combination rules for the LJ interaction between species i and j,

$$\epsilon_{ij} = \sqrt{\epsilon_i\epsilon_j} \quad \text{and} \quad \sigma_{ij} = \sqrt{\sigma_i\sigma_j}. \tag{19}$$

In the following, we always refer to the diagonal values $\epsilon_i \equiv \epsilon_{ii}$ and $\sigma_i \equiv \sigma_{ii}$, corresponding to the interaction parameters between identical atoms. Because all molecules that we use have only a single LJ site, we use the name of the molecule for the index i rather than the name of the atom. The LJ interactions are truncated at $r_c = 1.0$ nm using a shifted cutoff scheme, where a nonlinear function is added between $r = 0$ and $r = r_c$ to smoothen the interaction near r_c. We use a shifted cutoff because the simple LJ cutoff scheme may lead to artifacts when used in future nonequilibrium molecular dynamics simulations of electrokinetic flows.[48,49] For the Coulomb interactions, we employ a real-space cutoff length of 1.2 nm and particle mesh Ewald summation for larger separations, using cubic interpolations and a grid spacing of 0.12 nm for the reciprocal space sum, coupled with tinfoil boundary conditions. The temperature is fixed at 300 K and the pressure at 1 bar using the Berendsen thermostat and barostat, respectively. All distances within the ions are constrained using the SHAKE algorithm, and all distances within the water molecules using SETTLE. To avoid instabilities, we use a soft-core interaction potential for the LJ integration,[36,50]

$$V_{\mathrm{sc}}\left(r_{ij}\right) = (1-\lambda)\,V^0_{ij}\left(r^A_{ij}\right) + \lambda V^1_{ij}\left(r^B_{ij}\right), \tag{20}$$

where λ and V^λ_{ij} refer to the LJ part of the original potential defined in Eq. (6). The distances r^A_{ij} and r^B_{ij} are given by

$$r^A_{ij} = \left(\alpha\sigma_A^6\lambda^p + r_{ij}^6\right)^{\frac{1}{6}} \text{ and } r^B_{ij} = \left(\alpha\sigma_B^6(1-\lambda)^p + r_{ij}^6\right)^{\frac{1}{6}}, \tag{21}$$

where σ_A and σ_B refer to either the σ_{ij} value of the original LJ interaction, or an input parameter σ_{sc} when the original

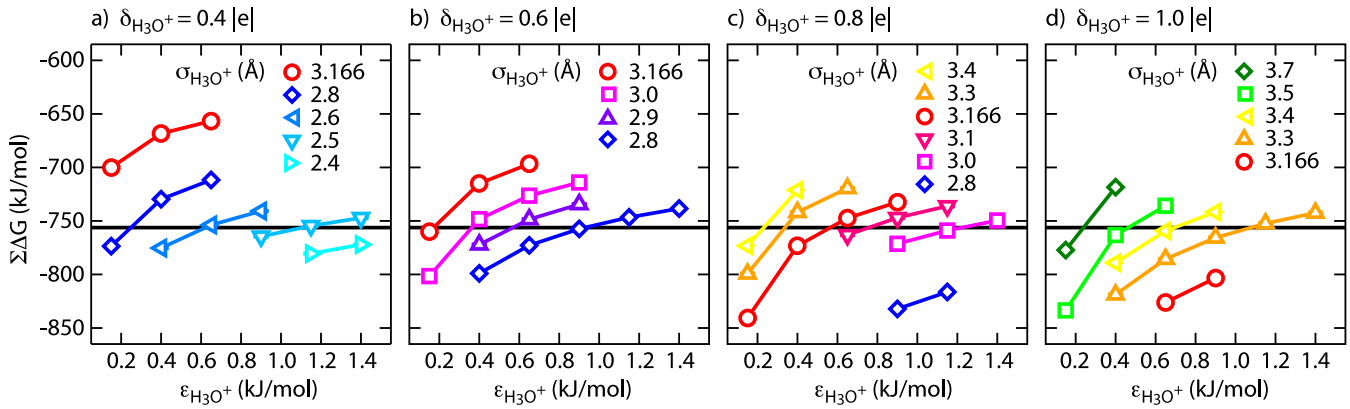

FIG. 2. The solvation free energy sum $\Sigma\Delta G$ for rigid H_3O^+ and Cl^- for different values of the partial charge $\delta_{H_3O^+}$ and the LJ parameters of the oxygen, $\epsilon_{H_3O^+}$ and $\sigma_{H_3O^+}$, compared with the experimental value (solid black line, Eq. (4)). The uncertainty in the simulation results is less than 0.4 kJ/mol.

value of σ_{ij} equals zero. We use $\sigma_{sc} = 0.3$ nm, $\alpha = 0.5$ and an exponent $p = 1$. Simulations are performed with a 2 fs time step. Simulation boxes are equilibrated for at least 2 ns, after which $\partial H/\partial\lambda$ is collected every 0.2 ps for 5 ns at every value of λ.

2. Kirkwood-Buff integration

The radial distribution functions $g_{\alpha\beta}(r)$ of the salt solutions are obtained from separate simulations performed in the NPT ensemble, at a pressure of 1 bar and temperature $T = 300$ K using Parrinello-Rahman and Nosé-Hoover coupling methods, respectively. The simulation box (a cubic box with sides of length $R = 4.5$ nm) contains 100 H_3O^+/OH^- and 100 Cl^-/Na^+ ions together with 5400 water molecules, which yields a solution with a concentration of 1.03 mol/l. For Na^+ and Cl^-, we use the Smith-Dang force fields summarized in Ref. 11, which reproduce the mean activity coefficient at a concentration of 0.3 mol/l, as well as the solvation free energy of Na^+Cl^- reasonably well. Note that there is no guarantee that the Kirkwood-Buff derived force fields,[13] which accurately reproduce the activity derivatives of Na^+Cl^- solutions, reproduce the solvation free energy equally well. The trajectory of the particles is written every 0.2 ps for a total simulation time of 100 ns, of which the first 10 ns is discarded for equilibration. Other simulation parameters are identical to the ones used for the thermodynamic integration. We calculate a_{cc} from Eq. (15) and $G^{\infty}_{\alpha\beta}$ by linearly extrapolating Eq. (17) to $1/R = 0$. We have verified our simulation method by reproducing the activity coefficient of Na^+Cl^- as a function of salt concentration using the force fields of Ref. 13 over the concentration range from 0.1 to 3.0 mol/l, showing excellent agreement with the experimental data and the original simulation results (data not shown).

V. RESULTS AND DISCUSSION

A. Solvation free energy

1. Chloride

The solvation free energy of the Smith-Dang Cl^-[51] depends slightly on the cutoff scheme used and on the value of the surface potential. Using $\psi_s = -0.527$ ($\Delta G_s = 50.8$ kJ/mol) and the simple LJ cutoff at 9 Å and long-range correction to the energy and pressure, we arrive at -307 ± 1 kJ/mol using AMBER and -305 ± 0.4 kJ/mol using GROMACS, comparing well with the value of -306 kJ/mol calculated by Horinek, Mamatkulov, and Netz.[10] Using $\psi_s = -0.546$ ($\Delta G_s = 52.7$ kJ/mol) and a shifted cutoff scheme at 10 Å without long-range correction, as we employ in our current work, we arrive at $\Delta G_{Cl^-} = -300.5 \pm 0.2$ kJ/mol. We have used an extra long simulation of 20 ns to calculate this value.

2. Hydronium

In Fig. 2, we plot the sum of the solvation free energies $\Sigma\Delta G$ for rigid H_3O^+ and Cl^- as a function of the LJ interaction strength $\epsilon_{H_3O^+}$ of the H_3O^+–H_3O^+ interaction. We show the free energy for different values of the partial charge $\delta_{H_3O^+}$ and

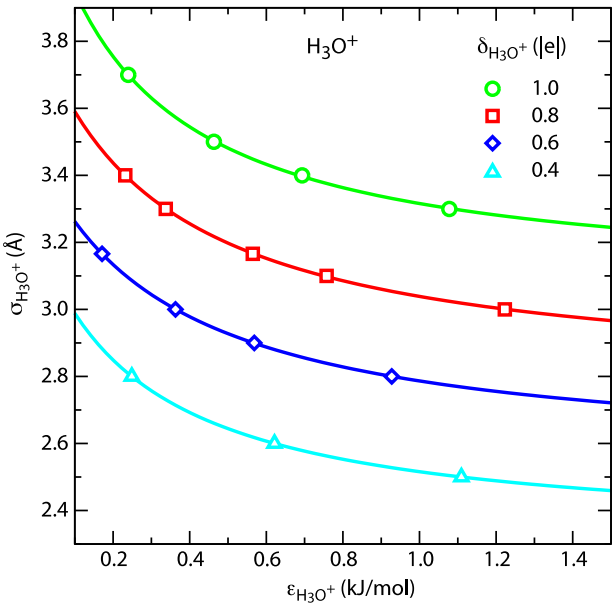

FIG. 3. Solvation free energy isolines of H_3O^+ in $\sigma_{H_3O^+}$—$\epsilon_{H_3O^+}$ space, extracted from Fig. 2. The solvation free energy sum $\Sigma\Delta G$ along the curves matches the experimental value of Eq. (4). The lines correspond to a fit of the heuristic function $(\epsilon_{H_3O^+} + A)(\sigma_{H_3O^+} + B) = C$, the parameters of which are listed in Table II.

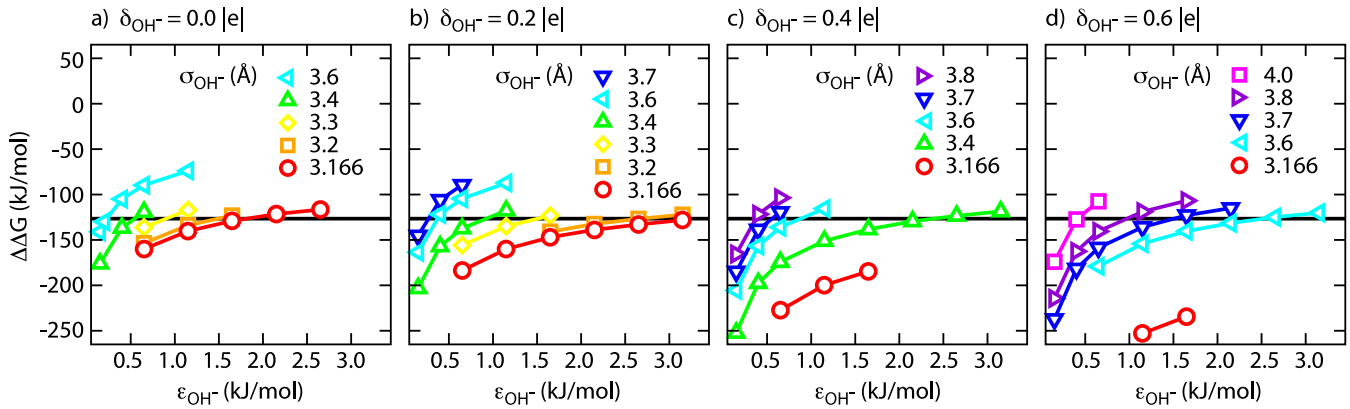

FIG. 4. The solvation free energy difference $\Delta\Delta G$ for OH^- and Cl^- for different values of the partial charge δ_{OH^-} and the LJ parameters of the oxygen, ϵ_{OH^-} and σ_{OH^-}, compared with the experimental value (solid black line, Eq. (4)). The uncertainty in the simulation results is less than 0.5 kJ/mol.

for different values of the LJ radius $\sigma_{H_3O^+}$, together with the experimental value of Eq. (4). The combinations of $\sigma_{H_3O^+}$ and $\epsilon_{H_3O^+}$ for which the solvation free energy sum $\Sigma\Delta G$ matches its experimental value are shown in Fig. 3 for different values of the partial charge $\delta_{H_3O^+}$.

3. Hydroxide

The difference of the free energy $\Delta\Delta G$ for OH^- and Cl^- is shown in Fig. 4 as a function of ϵ_{OH^-} of the OH^-–OH^- interaction. The combinations of σ_{OH^-} and ϵ_{OH^-} for which the solvation free energy difference $\Delta\Delta G$ matches the experimental value (Eq. (4)) are shown in Fig. 5 for different values of the partial charge δ_{OH^-}.

We fit the curves in Figs. 3 and 5 with the heuristic function $(\epsilon_i + A)(\sigma_i + B) = C$. The parameters A, B, and C are summarized in Table II for H_3O^+ and in Table III for OH^-.

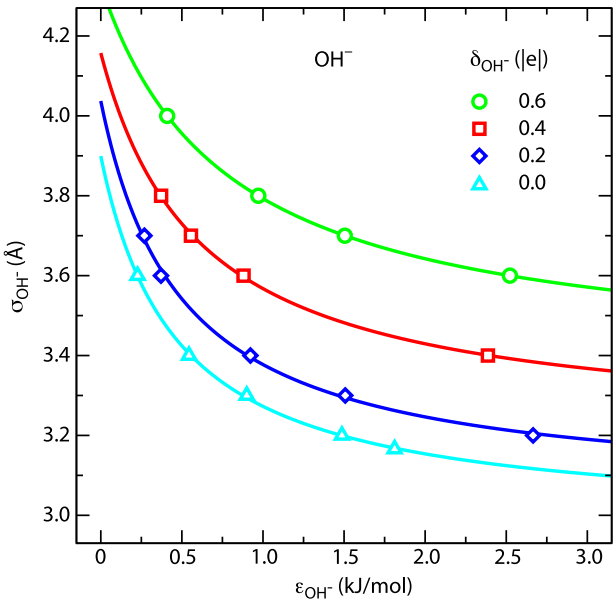

FIG. 5. Solvation free energy isolines of OH^- in σ_{OH^-}–ϵ_{OH^-} space, extracted from Fig. 4. The solvation free energy difference $\Delta\Delta G$ along the curves matches the experimental value of Eq. (4). Lines correspond to a fit of the heuristic function $(\epsilon_{OH^-} + A)(\sigma_{OH^-} + B) = C$ with the parameters given in Table III.

B. Activity derivatives

1. Hydronium

The log-log derivative a_{cc} of the activity of a 1.0 mol/l $H_3O^+Cl^-$ solution, calculated from Eq. (15), is shown in Fig. 6, together with the experimental values of Eq. (5). Because a_{cc} is calculated along the free energy isolines shown in Fig. 3, the value of $\sigma_{H_3O^+}$ varies along with $\epsilon_{H_3O^+}$ to keep the solvation free energy constant and equal to the experimental value. The curves for $\delta_{H_3O^+} = 0.8|e|$ and $\delta_{H_3O^+} = 1.0|e|$ cross the experimental line in the region $\epsilon_{H_3O^+} = 0.6 - 1.0$ kJ/mol, leading to several possible combinations of $\epsilon_{H_3O^+}$ and $\sigma_{H_3O^+}$. Interestingly, the curves for smaller partial charges do not reach the experimental activity derivative at all. We choose the LJ parameter combinations (a) $\epsilon_{H_3O^+} = 0.6$ kJ/mol, $\sigma_{H_3O^+} = 0.343$ nm at $\delta_{H_3O^+} = 1.0|e|$, (b) $\epsilon_{H_3O^+} = 0.8$ kJ/mol, $\sigma_{H_3O^+} = 0.31$ nm at $\delta_{H_3O^+} = 0.8|e|$, and (c) $\epsilon_{H_3O^+} = 1.0$ kJ/mol, $\sigma_{H_3O^+} = 0.332$ nm at $\delta_{H_3O^+} = 1.0|e|$ for further analysis. An excellent match between the simulation data and the experimental activity derivative of the $H_3O^+Cl^-$ solution is obtained for the LJ parameter combinations (b) of Fig. 6 ($\epsilon_{H_3O^+} = 0.8$ kJ/mol, $\sigma_{H_3O^+} = 0.31$ nm with $\delta_{H_3O^+} = 0.8|e|$)

TABLE II. Parameters of the function $(\epsilon_{H_3O^+} + A)(\sigma_{H_3O^+} + B) = C$, σ in Å, used to fit the solvation free energy isolines for H_3O^+ in Fig. 3.

$\delta_{H_3O^+}$ ($\|e\|$)	A	B	C
0.4	0.282 865	−2.314 66	0.258 036
0.6	0.358 120	−2.544 38	0.328 952
0.8	0.331 164	−2.774 38	0.351 967
1.0	0.256 339	−3.065 91	0.314 208

TABLE III. Parameters of the function $(\epsilon_{OH^-} + A)(\sigma_{OH^-} + B) = C$, σ in Å, used to fit the solvation free energy isolines for OH^- in Fig. 5.

δ_{OH^-} ($\|e\|$)	A	B	C
0.0	0.468 548	−2.979 14	0.431 134
0.2	0.496 065	−3.050 08	0.489 751
0.4	0.611 913	−3.206 60	0.581 816
0.6	0.783 927	−3.373 83	0.747 371

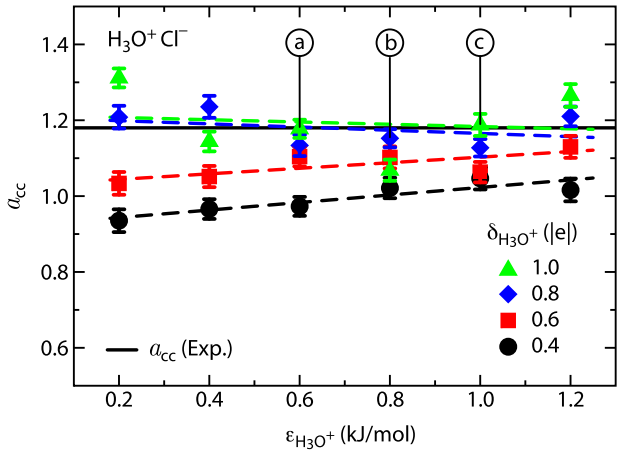

FIG. 6. Activity coefficient derivative (Eq. (15)) of the 1 mol/l $H_3O^+Cl^-$ electrolyte as a function of the LJ parameters that lie on the solvation free energy isoline (Fig. 3) for different partial charge distributions on atoms. For H_3O^+, the LJ diameter is varied between $\sigma_{H_3O^+} = 0.25$ nm and $\sigma_{H_3O^+} = 0.38$ nm. Satisfactory matches between the simulated and the experimental activity derivative (solid line, $a_{cc} = 1.18$) are obtained at (a) $\delta_{H_3O^+} = 1.0|e|$ and $\epsilon_{H_3O^+} = 0.6$ kJ/mol, $\sigma_{H_3O^+} = 0.343$ nm; (b) $\delta_{H_3O^+} = 0.8|e|$ and $\epsilon_{H_3O^+} = 0.8$ kJ/mol, $\sigma_{H_3O^+} = 0.310$ nm; and (c) $\delta_{H_3O^+} = 1.0|e|$ and $\epsilon_{H_3O^+} = 1.0$ kJ/mol, $\sigma_{H_3O^+} = 0.332$ nm.

over a wide range of concentrations, as we show in the top panel of Fig. 7. In contrast to the curve for $\delta_{H_3O^+} = 0.8|e|$, the activity derivative for a partial charge of $\delta_{H_3O^+} = 1.0|e|$—which works well at $n = 1.0$ mol/l by construction—deviates from the experimental line for high and low concentrations for both parameter combinations (a) and (c) of Fig. 6 (bottom panel of Fig. 7). As the system is underdetermined, we expect good results for a limited set of parameters close to those of the optimized force field. However, given the sensitivity of the thermodynamic properties to $\delta_{H_3O^+}$ in particular, we can restrict the possible partial charges to $\delta_{H_3O^+} = 0.8 \pm 0.1|e|$.

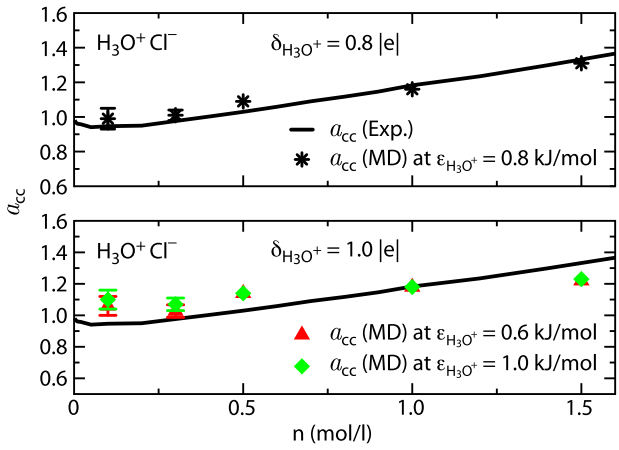

FIG. 7. Activity coefficient derivative (Eq. (15)) of the $H_3O^+Cl^-$ electrolyte as a function of the salt concentration. Error bars are only shown when larger than the symbol size. Activity derivatives are calculated at $\delta_{H_3O^+} = 0.8|e|$ for $\epsilon_{H_3O^+} = 0.8$ kJ/mol, $\sigma_{H_3O^+} = 0.310$ nm (black stars, (b) in Fig. 6); at $\delta_{H_3O^+} = 1.0|e|$ for $\epsilon_{H_3O^+} = 0.6$ kJ/mol, $\sigma_{H_3O^+} = 0.343$ nm (red triangles, (a) in Fig. 6); and at $\delta_{H_3O^+} = 1.0|e|$ for $\epsilon_{H_3O^+} = 1.0$ kJ/mol, $\sigma_{H_3O^+} = 0.332$ nm (green diamonds, (c) in Fig. 6). The best match between the simulation data and the experimental activity derivative of the $H_3O^+Cl^-$ solution is obtained for the LJ parameters $\epsilon_{H_3O^+} = 0.8$ kJ/mol, $\sigma_{H_3O^+} = 0.310$ nm (black stars) with $\delta_{H_3O^+} = 0.8|e|$ (upper panel).

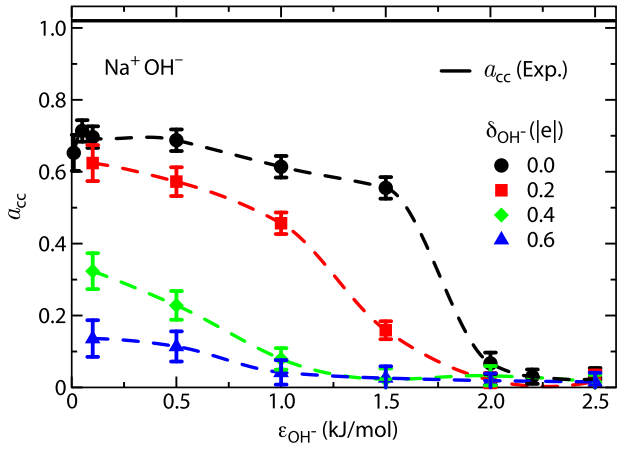

FIG. 8. Activity coefficient derivative (Eq. (15)) of a 1.0 mol/l Na^+OH^- solution as a function of LJ parameters that lie on the solvation free energy isoline (Fig. 5) and partial charge distribution on atoms. For OH^-, the LJ diameter is varied between $\sigma_{OH^-} = 0.3$ nm and $\sigma_{OH^-} = 0.43$ nm. The horizontal solid line denotes the corresponding experimental activity derivative value of Na^+OH^- at 1 mol/l ($a_{cc} = 1.02$). For further optimization, we choose $\delta_{OH^-} = 0$ and the LJ parameter combination of $\epsilon_{OH^-} = 0.05$ kJ/mol, $\sigma_{OH^-} = 0.381$ nm, which gives an activity derivative closest to the experimental value.

2. Hydroxide

We show the log-log derivative a_{cc} of the activity of a 1.0 mol/l Na^+OH^- solution in Fig. 8. Clearly, the LJ parameter combinations that reproduce the OH^- and Na^+ solvation free energies fail to reproduce the experimental activity coefficient derivatives of a Na^+OH^- solution. To overcome this problem, we follow a recently proposed scheme, which modifies the combination rule for the cation-anion effective radius, and was used to reproduce the experimental activity derivatives of monovalent and divalent salt solutions.[11,12] Such a procedure makes sense, since the standard combination rules of Eq. (19) are completely heuristic, and there is *a-priori* no reason why they should work for every combination of atoms.

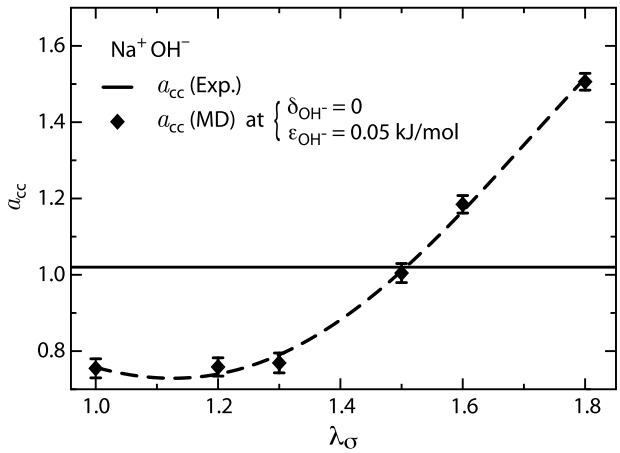

FIG. 9. The activity derivative (Eq. (15)) as a function of the scaling prefactor λ_σ at 1 mol/l of Na^+OH^-. The symbols show the simulation results, the dashed curve is a fourth-order polynomial fitting function to guide the eye. We use $\delta_{OH^-} = 0$ and the LJ parameters $\epsilon_{OH^-} = 0.05$ kJ/mol, $\sigma_{OH^-} = 0.381$ nm at $\delta_{OH^-} = 0|e|$ for OH^-, together with the Smith-Dang parameters for Na^+.[11] The horizontal solid line denotes the corresponding experimental activity derivative $a_{cc} = 1.02$ of Na^+OH^- at 1 mol/l.

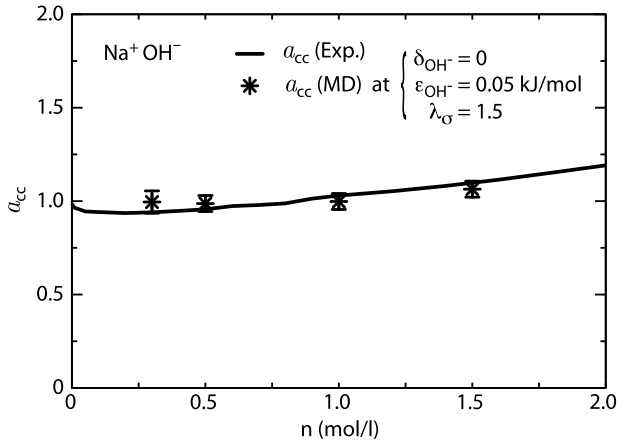

FIG. 10. The activity derivative (Eq. (15)) as a function of the Na^+OH^- concentration. The symbols show the simulation results, the curve denotes the experimental activity derivative.[31–33] We use the LJ parameters $\epsilon_{OH^-} = 0.05$ kJ/mol, $\sigma_{OH^-} = 0.381$ nm, and the Smith-Dang sodium parameters with a scaling prefactor of $\lambda_\sigma = 1.5$.

Therefore, to modify the activity without changing the single-ion solvation free energies, a freely adjustable scaling factor λ_σ is introduced in the cation-anion effective radius

$$\sigma_{+-} = \lambda_\sigma \sqrt{\sigma_+ \sigma_-}. \tag{22}$$

TABLE IV. Non-bonded interaction parameters used in the simulations with final LJ parameters and partial charges q obtained in this work for Na^+OH^- and $H_3O^+Cl^-$ salt solutions. The geometric combination rules are used for σ_{ij} and ϵ_{ij} (Eq. (19)), and the LJ radius for the OH^-–Na^+ interaction is modified according to Eq. (22) with $\lambda_\sigma = 1.5$. The parameters for $i = j$ are denoted by σ_i and ϵ_i.

Sites	σ_i (nm)	ϵ_i (kJ/mol)	q ($\lvert e \rvert$)	Reference
O (H_3O^+)	0.31	0.8	−1.4	This work
H (H_3O^+)	0	0	0.8	This work
O (OH^-)	0.381	0.05	−1.0	This work
H (OH^-)	0	0	0	This work
Na^+	0.261	0.4186	1	11
Cl^-	0.452	0.4186	−1	11
O (H_2O)	0.3166	0.65	−0.8476	7
H (H_2O)	0	0	0.4238	7

The cation-cation, anion-anion, and water-ion combination rules are not modified.

We choose the lowest possible partial charge, $\delta_{OH^-} = 0$ and $\epsilon_{OH^-} = 0.05$ kJ/mol, which gives the best results for a_{cc} (Fig. 8). The cation-anion scaling prefactor λ_σ is varied in discrete steps, $\lambda_\sigma \in \{1.0, 1.2, 1.3, 1.5, 1.6, 1.8\}$. In Fig. 9, we show the activity derivatives a_{cc} as a function of the scaling prefactor λ_σ at a concentration of Na^+OH^- of 1.0 mol/l. The

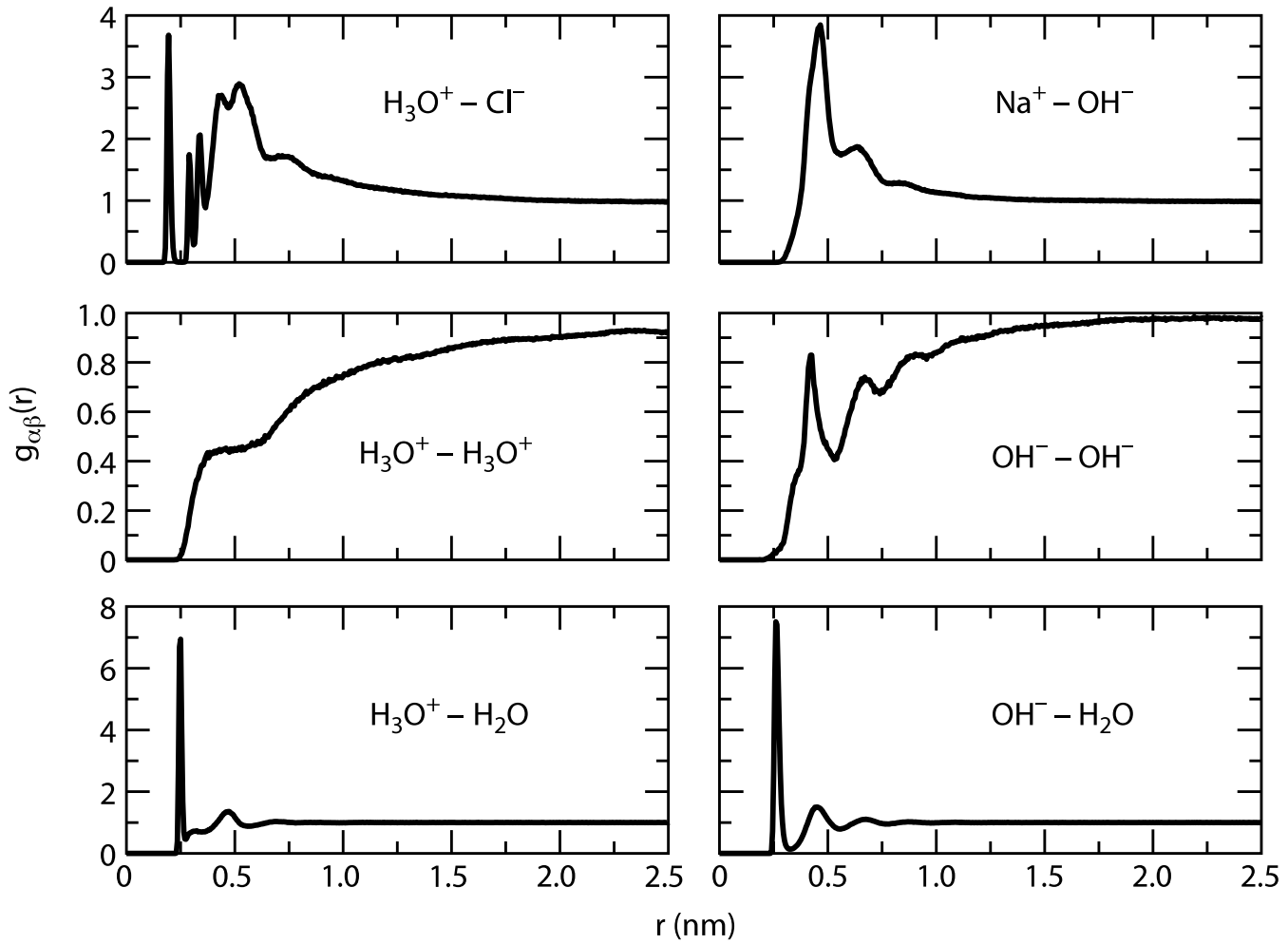

FIG. 11. The radial distribution functions $g_{\alpha\beta}(r)$, where α and β refer to the ions and the water molecules, of $H_3O^+Cl^-$ and Na^+OH^- solutions at a concentration of $n = 1$ mol/l. For H_3O^+, OH^-, and H_2O, we use the position of the oxygen atom to calculate $g_{\alpha\beta}(r)$.

experimental value for a_{cc} (Eq. (5)) is denoted by a horizontal line. The symbols show the simulated activity derivatives and the dashed line denotes a fourth-order polynomial fit. A match between the simulated and the experimental activity derivatives for Na^+OH^- is obtained at $\lambda_\sigma = 1.5$. Using this value, we reproduce the activity derivatives of Na^+OH^- solutions well in a wide concentration range (Fig. 10), validating our newly developed force field.

In Table IV, we summarize the results of our force field optimization, together with the parameters of Na^+, Cl^-, and SPC/E water. The radial distribution functions of the $H_3O^+Cl^-$ and Na^+OH^- solutions, using the optimized force field parameters of Table IV at a concentration of $n = 1$ mol/l, are shown in Fig. 11.

C. Comparison with experimental data and quantum chemistry

To test the performance of the new force fields, we compare the static dielectric constant and the mass density of Na^+OH^- and $H_3O^+Cl^-$ solutions as a function of the ionic concentration with experimental data[52,53] (Fig. 12). We calculate the static dielectric constant from the fluctuations of the total dipole moment, which is accurate for bulk systems.[40] The dielectric constant decreases as a function of the concentration and the dielectric decrement agrees well with the experimental data (Fig. 12(a)). Note that the dielectric constant of the SPC/E water model is lower than the experimental value of pure water,[39] so our simulation results are shifted with respect to the experimental data by a roughly constant value.

The new force fields also correctly reproduce the increasing mass density as a function of ion concentration, showing a significantly stronger increase for Na^+OH^- than for $H_3O^+Cl^-$, in agreement with the experimental data (Fig. 12(b)); whereas the mass density increment of Na^+OH^- solutions is overestimated, the density of $H_3O^+Cl^-$ solutions follows the experimental data very accurately.

Quantum chemical calculations of the charge distribution on H_3O^+ molecules consistently indicate a lower value of $\delta_{H_3O^+}$, see Table I. One example of a quantum chemistry optimized H_3O^+ molecule[6] has a lower dipole moment ($P_z = 0.037\,e$ nm) and a larger diagonalized traceless quadrupole moment ($Q_{xx} = Q_{yy} = 0.11\,e$ nm^2 and $Q_{zz} = -0.23\,e$ nm^2) than our optimized force field ($P_z = 0.066\,e$ nm, $Q_{xx} = Q_{yy} = 0.002\,e$ nm^2, $Q_{zz} = -0.003\,e$ nm^2), all with respect to the center of mass. However, it is important to realize that the thermodynamics of the solvated proton originate in the properties of a mixture of hydrated proton complexes, such as the hydronium (H_3O^+), the Zundel ($H_5O_2^+$), and the Eigen ($H_9O_4^+$) forms, which may have different charge distributions. The electrostatic moments of the quantum chemistry optimized Zundel ion,[6] for example, are much closer to the values of our new force field ($P_z = 0.066\,e$ nm, $Q_{xx} = 0.010\,e$ nm^2, $Q_{yy} = -0.001\,e$ nm^2, $Q_{zz} = -0.009\,e$ nm^2). Consequently, a quantum chemical calculation of hydronium does not necessarily yield electrostatic moments that are consistent with thermodynamics when used in conjunction with a nonpolarizable force field. In fact, as can be

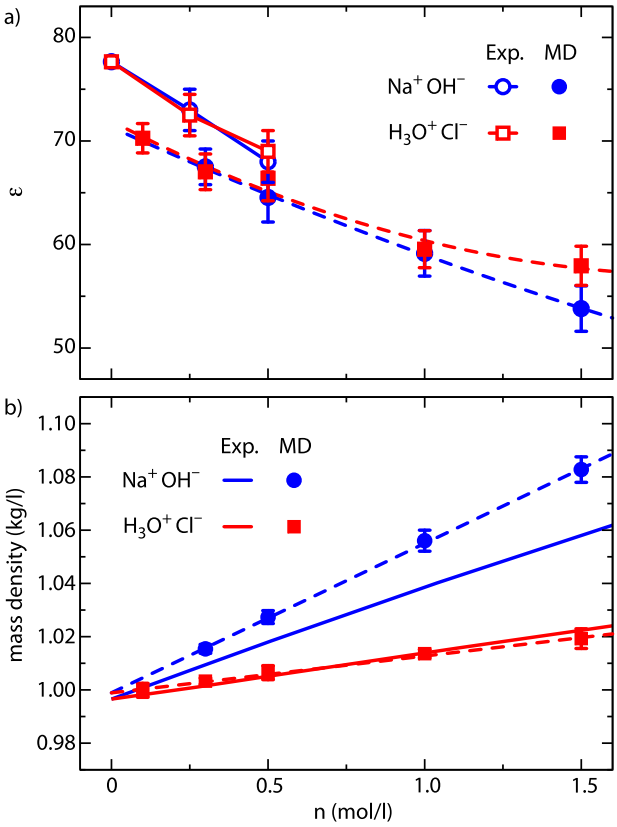

FIG. 12. The static dielectric constant (a) and mass density (b) of simulated $H_3O^+Cl^-$ and Na^+OH^- solutions as a function of the ion concentration (solid symbols). The open symbols and solid lines correspond to experimental data from Refs. 52 (a) and 53 (b), and the dashed lines are drawn as a guide to the eye.

derived from Figs. 2 and 6, the force field parameters referenced in Table I fail to reproduce the experimental solvation free energy, the activity derivative, or both. For example, the rigid nonpolarizable H_3O^+ force field of Ref. 22 ($\sigma_{H_3O^+} = 0.29$ nm, $\epsilon_{H_3O^+} = 1.15$ kJ/mol, $\delta_{H_3O^+} = 0.416|e|$), which has a value of $\delta_{H_3O^+}$ which is typical for quantum chemistry optimized force fields, yields a solvation free energy sum of $\Sigma\Delta G_{H_3O^+} = -679.9 \pm 0.3$ kJ/mol (in SPC/E water, with Cl^- as the reference ion), which is 76.4 kJ/mol higher than the experimental value. In some sense, one might say that our optimized force field parameters compensate for the neglect of polarizability and other multi-body effects—as indeed any correctly parameterized nonpolarizable force field does.

The thermodynamically consistent OH^- ion does not have a dipole moment at all. Although surprising at the first sight, this result is supported by recent small-angle x-ray scattering experiments, showing that the wave vector-dependent structure factor of Na^+OH^- solutions resembles that of Na^+F^- solutions.[54]

VI. CONCLUSIONS

We have developed nonpolarizable hydronium and hydroxide ion force fields, to be used in conjunction with the SPC/E water model, through molecular dynamics simulations. The parameters of the force fields are optimized with respect

to the experimental solvation free energies and the activities of Na^+OH^- and $H_3O^+Cl^-$ salt solutions. Our optimization thus ensures that the properties of both water-ion interactions and ion pairing are reproduced in accordance with experimental findings. The obtained models for Na^+OH^- and $H_3O^+Cl^-$ allow for precise molecular dynamics simulations of the relative distribution of these ions in aqueous salt solutions, accurately reproducing their experimental solvation free energies and solution activities over a wide range of concentrations. Having such thermodynamically consistent force fields is important not only for simulating electrolyte solutions but also for studying the effects of ions on larger solutes.[55,56] Both the solvation free energy and the degree of anion-cation aggregation are very sensitive to the partial charge on the hydrogen atoms of H_3O^+ and OH^-. For H_3O^+, the partial charge of the new force field is significantly higher than the one used for the hydrogen of water and significantly higher than the one employed in the most commonly used H_3O^+ force fields from the literature. In contrast to H_3O^+, the partial charge of the new OH^- force field exhibits the opposite trend. In fact, in order to reproduce the activity derivatives for Na^+OH^-, the partial charge needs to be set to zero, in addition to a modification of the anion-cation LJ combination rule. The strong deviations of the force field parameters from previous force field models might provide an explanation for the generally poor comparison with experimental data that have been obtained with previous force fields. Comparisons with experimental data for observables that have not been used in the optimization, specifically with the dielectric decrement and the mass density, show good agreement, suggesting that the optimized force fields are transferable to different settings. Our results show that, generally speaking, polarizability is not necessary to create thermodynamically consistent force field models. With this optimization, we have obtained a force field for the water ions that treats both the electrostatic and the short-ranged interactions on the same level as the highly successful, rigid, nonpolarizable, simple point charge models for water.

ACKNOWLEDGMENTS

Sh.I.M. acknowledges financial support from the DAAD Fellowship and State S&T program of the Republic of Uzbekistan (No. KA-4-002). R.R.N. acknowledges support from the DFG as part of the SFB 1078 "Protonation Dynamics in Protein Function." D.J.B. acknowledges funding from the Glasstone Benefaction and Linacre College. We gratefully acknowledge the HPC cluster at ZEDAT, Freie Universität Berlin, for computing time.

[1]T. F. Tadros and J. Lyklema, J. Electroanal. Chem. **17**, 267 (1968).
[2]B. Honig and A. Nicholls, Science **268**, 1144 (1995).
[3]N. Lane and W. F. Martin, Cell **151**, 1406 (2012).
[4]J. K. Beattie, A. M. Djerdjev, and G. G. Warr, Faraday Discuss. **141**, 31 (2009).
[5]V. Buch *et al.*, Proc. Natl. Acad. Sci. U. S. A. **104**, 7342 (2007).
[6]R. Vácha, V. Buch, A. Milet, J. P. Devlin, and P. Jungwirth, Phys. Chem. Chem. Phys. **9**, 4736 (2007).
[7]H. J. C. Berendsen, J. R. Grigera, and T. P. Straatsma, J. Phys. Chem. **91**, 6269 (1987).
[8]F. Sedlmeier, D. Horinek, and R. R. Netz, J. Am. Chem. Soc. **133**, 1391 (2011).
[9]S. Gekle and R. R. Netz, J. Chem. Phys. **137**, 104704 (2012).
[10]D. Horinek, S. I. Mamatkulov, and R. R. Netz, J. Chem. Phys. **130**, 124507 (2009).
[11]M. Fyta and R. R. Netz, J. Chem. Phys. **136**, 124103 (2012).
[12]S. Mamatkulov, M. Fyta, and R. R. Netz, J. Chem. Phys. **138**, 024505 (2013).
[13]S. Weerasinghe and P. E. Smith, J. Chem. Phys. **119**, 11342 (2003).
[14]B. Klasczyk and V. Knecht, J. Chem. Phys. **132**, 024109 (2010).
[15]B. Hess and N. F. A. Van der Vegt, Proc. Natl. Acad. Sci. U. S. A. **106**, 13296 (2009).
[16]D. E. Sagnella and G. A. Voth, Biophys. J. **70**, 2043 (1996).
[17]W. Chen, J. A. Wallace, Z. Yue, and J. K. Shen, Biophys. J. **105**, L15–L17 (2013).
[18]J. S. Hub, M. G. Wolf, C. Caleman, P. J. van Maaren, G. Groenhof, and D. van der Spoel, Chem. Sci. **5**, 1745 (2014).
[19]B. Temelso, T. Köddermann, K. N. Kirschner, K. Klein, and G. C. Shields, Comput. Theor. Chem. **1021**, 240 (2013).
[20]R. Vácha, D. Horinek, M. L. Berkowitz, and P. Jungwirth, Phys. Chem. Chem. Phys. **10**, 4975 (2008).
[21]S. S. Jang, V. Molinero, T. Çağın, and W. A. Goddard III, J. Phys. Chem. B **108**, 3149 (2004).
[22]I. Kusaka, Z.-G. Wang, and J. H. Seinfeld, J. Chem. Phys. **108**, 6829 (1998).
[23]Y. Marcus, *Ion Properties* (CRC Press, 1997).
[24]M. D. Tissandier *et al.*, J. Phys. Chem. A **102**, 7787 (1998).
[25]M. W. Chase, *NIST-JANAF Thermochemical Tables*, 4th ed., Journal of Physical and Chemical Reference Data Monograph No. 9 (American Chemical Society/American Institute of Physics, 1998).
[26]J. E. Szulejko and T. B. McMahon, J. Am. Chem. Soc. **115**, 7839 (1993).
[27]J. R. Pliego and J. M. Riveros, Chem. Phys. Lett. **332**, 597 (2000).
[28]D. M. Camaioni and C. A. Schwerdtfeger, J. Phys. Chem. A **109**, 10795 (2005).
[29]W. Wagner and A. Pruss, J. Phys. Chem. Ref. Data **22**, 783 (1993).
[30]J. R. Pliego and J. M. Riveros, J. Phys. Chem. B **104**, 5155 (2000).
[31]H. S. Harned and B. B. Owen, *Physical Chemistry of Electrolyte Solutions*, 3rd ed. (Reinhold Publishing Corp., 1963).
[32]W. J. Hamer and Y. Wu, J. Phys. Chem. Ref. Data **1**, 1047 (1972).
[33]R. A. Robinson and R. H. Stokes, *Electrolyte Solutions*, 2nd ed. (Dover, New York, 2002).
[34]P. A. Kollman and C. F. Bender, Chem. Phys. Lett. **21**, 271 (1973).
[35]T. J. Sears, P. R. Bunker, P. B. Davies, S. A. Johnson, and V. Spirko, J. Chem. Phys. **83**, 2676 (1985).
[36]B. Hess, C. Kutzner, D. van der Spoel, and E. Lindahl, J. Chem. Theory Comput. **4**, 435 (2008).
[37]P. H. Hünenberger and J. A. McCammon, J. Chem. Phys. **110**, 1856 (1999).
[38]B. R. A. Nijboer and T. W. Ruijgrok, J. Stat. Phys. **53**, 361 (1988).
[39]D. J. Bonthuis, S. Gekle, and R. R. Netz, Phys. Rev. Lett. **107**, 166102 (2011).
[40]D. J. Bonthuis, S. Gekle, and R. R. Netz, Langmuir **28**, 7679 (2012).
[41]G. Lee Warren and S. Patel, J. Chem. Phys. **127**, 064509 (2007).
[42]V. P. Sokhan and D. J. Tildesley, Mol. Phys. **92**, 625 (1997).
[43]F. Sedlmeier, J. Janeček, C. Sendner, L. Bocquet, R. R. Netz, and D. Horinek, Biointerphases **3**, FC23 (2008).
[44]M. R. Shirts, D. L. Mobley, J. D. Chodera, and V. S. Pande, J. Phys. Chem. B **111**, 13052 (2007).
[45]P. G. Kusalik and G. N. Patey, J. Chem. Phys. **86**, 5110 (1987).
[46]J. G. Kirkwood and F. P. Buff, J. Chem. Phys. **19**, 774 (1951).
[47]P. Krüger, S. K. Schnell, D. Bedeaux, S. Kjelstrup, T. J. H. Vlugt, and J. Simon, J. Phys. Chem. Lett. **4**, 235 (2013).
[48]D. J. Bonthuis, K. Falk, C. N. Kaplan, D. Horinek, A. N. Berker, L. Bocquet, and R. R. Netz, Phys. Rev. Lett. **105**, 209401 (2010).
[49]D. J. Bonthuis, D. Horinek, L. Bocquet, and R. R. Netz, Langmuir **26**, 12614 (2010).
[50]T. C. Beutler, A. E. Mark, R. C. van Schaik, P. R. Gerber, and W. F. van Gunsteren, Chem. Phys. Lett. **222**, 529 (1994).
[51]L. X. Dang and D. E. Smith, J. Chem. Phys. **99**, 6950 (1993).
[52]J. B. Hasted, D. M. Ritson, and C. H. Collie, J. Chem. Phys. **16**, 1 (1948).
[53]R. H. Perry and D. W. Green, *Perry's Chemical Engineers' Handbook*, 6th ed. (McGraw-Hill, New York, 1984).
[54]C. Chen *et al.*, J. Chem. Phys. **138**, 154506 (2013).
[55]P. E. Smith, J. Phys. Chem. B **108**, 18716 (2004).
[56]M. M. Reif, M. Winger, and C. Oostenbrink, J. Chem. Theory Comput. **9**, 1247 (2013).